This paper appears in Smart Materials and Structures 2013
doi:10.1088/0964-1726/23/2/025028
http://www.iopscience.iop.org/0964-1726/23/2/025028/

Development of a multilayered wide-ranged torque magnetorheological brake

Carlos Rossa, Adrien Jaegy, Alain Micaelli, and José Lozada

Abstract—**This paper presents the design of a multilayered magnetorheological brake from modelling to prototyping and characterisation. A magnetostatic model intended to provide a specific magnetic flux density over a fluid gap regardless of the dimensions of the fluid surface is proposed. The ferromagnetic path and the coil are dimensioned in consequence. The model needs only three inputs to completely define the brake i.e. the number of fluid gaps, the inner radius of the smallest fluid gap and the fluid gap depth. The evaluation criteria are defined by the torque density, the controllability and the reactivity, described as a function of the dimensions and the number of fluid gaps. The model has been optimized to improve the torque density. The brake has 4 fluid gaps and has been built and characterized. The expected torque when the fluid reaches the desired induction is 3.4 Nm and the measured torque is 3.6 Nm. This represents a relative error of 5.5%. The brake has 60 mm diameter, 39 mm width with a hollow shaft of 12 mm diameter. When exploited up to complete saturation, the measured torque is 5.3 Nm with 19 W power consumption. The brake has a torque density of 48.1 kN/m^2, a maximum-to-minimum torque ratio of 176 with 50 ms electromechanical time constant.**

I. INTRODUCTION

Rheological fluids have been successfully applied in a wide range of high fidelity actuators within the context of human-machine interfaces during the past two decades. Such devices provide fast response time, high force per volume ratio with low power requirements, making them particularly suitable for the design of embedded systems [18].

A rheological fluid consists of a suspension of micron-sized soft ferromagnetic or non-conducting particles dispersed in a carrying liquid (typically mineral oils, synthetic oils or water). Their rheological properties can be instantly, strongly and reversibly modified by the action of an electric field, in the case of a electrorheological fluid (ERF) [4], or by the action of a magnetic field in the case of a magnetorheological fluid (MRF) [13]. While ERF-based actuators typically need excitation voltages in the range of a kilovolt, MRF-based actuators need relatively low operating currents and voltages.

Designing an MRF actuator implies dealing with non-linearities introduced by the fluid behaviour and the magnetic saturation. Furthermore, a tradeoff can be observed between the measures of performance characterizing an MRF actuator. For human friendly robotics applications, the actuator can be evaluated with regards to the torque density, controllability and reactivity. Torque density ρ is the ratio torque-to-volume in terms of N/m^2, the controllability K is the maximum torque to minimum torque ratio, and the reactivity δt is the torque-to-eletric time constant ratio in terms of Nm/s measured for a step-type excitation.

Most of the available work dealing with the design and optimization of MRF actuators predominantly focusses on torque optimization. For instance, Karakoc et al. [7] present the design of an automotive MRF brake using a multiphysics optimization method to maximize the controllable torque. A cost function is defined including the braking torque and weight. In the same way, using finite element analysis, Park et al. [16] define cost functions to maximize to the torque-to-weight ratio while keeping a minimal required braking torque. Gudmundsson et al. [5] present a multi-objective optimization method for a prosthetic knee brake in terms of controllable torque, including also the off-state torque and weight. They consider an optimization parameter as a constraint in the modelling, or as an additional objective function. Zhang et al. [24] focus on a finite element analysis of the magnetic circuit saturation of an MRF-based damper. Yang et al. [23] investigate the feasibility of an MRF valve considering the relation of the volume fraction to yield stress, response time of the coils and electric power losses. Nguyen et al. [14] present an optimized design of a motorcycle brake where the required braking torque, temperature, mass and geometric dimensions are defined as optimization constraints. In some approaches, the goal of the optimization is to increase the magnetic flux in the MRF as much as possible [1]. However, the necessary coil volume and power supply increase considerably if the fluid becomes saturated.

With regards to the considered evaluation criteria, a commercially available MRF-brake (RD-2078-01) from Lord Corporation [2] has 96.6 mm diameter, 35.7 mm width and generates from 0.4 Nm (off-state torque) to 4 Nm at 1 A. The response time is 10 ms, yielding a torque density of 12.5 kN/m^2, a controllability of 10, and a reactivity of 400 Nm/s. Liu et al. [11] discus the conception of a single disc MRF brake able to provide 0.5 to 7 Nm at 2 A, or rather a torque density of 17.4 kN/m^2, and a dynamic range of 14. Guo and Liao [6] present the optimization of a clutch/brake system and obtain a torque density of 13.6 kN/m^2, and a reactivity ratio of 19.2 Nm/s. Senkal and Gurocak [22] present the design of a 10.9 Nm serpentine flux path-based brake with low friction sealing technique in order to reduce off-state torque. The authors present a o torque density of 38.4 kN/m^2, a controllability of 109, and a reactivity of 181.2 Nm/s.

This paper presents the design of a high torque density MRF brake from analytical modelling to prototyping and characterisation. A magnetostatic model intended to deliver a desired magnetic flux density over the fluid surface is

---

The authors are with the French Atomic Energy Commission, CEA, LIST Sensorial and Ambient Interfaces Laboratory 91191 Gif-sur-Yvette, France. Email: rossa@ualberta.ca; joselozada@uti.edu.ec; alain.micaelli@cea.fr

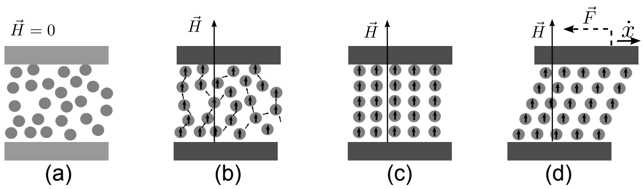

Fig. 1. Rheological effect in an MRF suspension between shearing plates. The particles are homogeneously distributed in the carrier liquid (a). A magnetic field $\vec{H}$ is applied and magnetizes the particles which behave as a magnetic dipole and undergo interaction forces (b) before forming chain-like structures aligned to the field (c). A relative displacement of the poles stretches the chains and create a resistive force $\vec{F}$ against the velocity $\dot{x}$ (d). The resistive force increases with the magnitude of the applied magnetic field.

developed. The model allows for an optimal design of the ferromagnetic path and the coil taking into consideration the magnetic saturation. It also defines the mentioned evaluation criteria as a function of the dimensions and the number of fluid gaps. The design requirements are: a desired torque of 3.2 Nm, an external radius inferior to 30 mm and a 6 mm radius hollow shaft. The paper is organized as follows. Section II presents a brief review of the MRF behaviour. The brake geometry and its respective magnetostatic model are subsequently presented and the evaluation criteria are defined. In Section III, the linear range of the analytical model is verified using finite element analysis. The results highlight that the evaluation criteria are interconnected and a compromise between torque density and controllability must be found. The optimized brake has been built and the experimental results are presented in Section IV. The final dimensions are 60 mm diameter, 39 mm width with a hollow shaft of 12 mm diameter. The torque varies from 0.03 Nm to 5.3 Nm and the brake consumes 19 W. This gives a torque density of 48.1 kN/m^2, a controllability of 176.6 and a reactivity ratio of 106 Nm/s.

II. ANALYTICAL MODELLING

In this section the analytical model based on the Bingham plastic formulation is developed. The model defines the evaluation criteria as a function of the dimensions and the number of fluid gaps.

A. Rheological Behaviour

Fig. 1 shows the rheological effect in an MR suspension and how this principle can be employed for the design of MRF-based actuators. The fluid is commonly confined between two magnetic poles. In the absence of a magnetic field, the particles of the MR suspension are homogeneously distributed in the carrier fluid and the suspension behaves as a Newtonian fluid Fig.1(a). When a magnetic field $\vec{H}$ is applied, the particles are magnetized and undergo magnetic interaction forces Fig.1(b). Hence, they form chain-like structures or aggregates aligned roughly parallel to the applied field Fig.1(c). The chain structures create a mechanical resistance against the relative motion of the poles or against a fluid flow. This phenomenon is macroscopically perceived as an almost instantaneous alteration of the fluid's apparent viscosity. When the mangetic poles are displaced, a resistive force appears on the poles passing through them, slowing or stopping their relative displacement Fig.1(d). This phenomenon can be exploited to the design of controllable brakes.

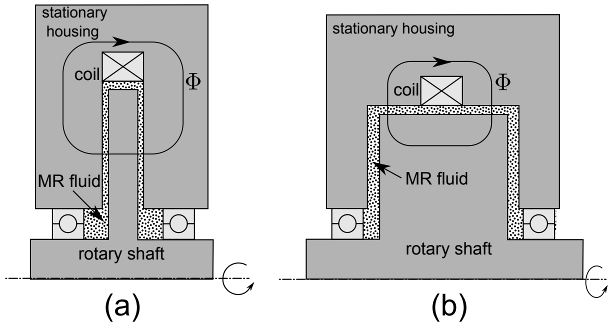

(a) (b)

Fig. 2. Single disc (a) and single cylinder (b) based brakes. The disc brake is composed of a thin fluid gap perpendicular to the rotation axis. In the cylindrical brake the fluid is in a cylindrical volume around the axis. The magnetic flux Φ is provided by a coil.

The Bingham model [10] is commonly used to describe the behaviour of MRFs as a function of the magnetic field H. The fluid shear stress $\tau(\dot{\gamma},H)$ delivered by the fluid is considered as a contribution of both a field dependent yield stress $\tau_y(H)$ and a viscous friction, which is dependent on the shear stress rate $\dot{\gamma}$ and the fluid viscosity η. The Bingham formulation gives:

$$|\tau(\dot{\gamma},H)| = \tau_y(H) + \eta|\dot{\gamma}| \quad if\, |\tau(\dot{\gamma},H)| \geqslant \tau_y(H) \tag{1}$$

$$\dot{\gamma} = 0 \qquad otherwise \tag{2}$$

By setting the magnetic field strength, the fluid can display a controllable yield stress.

B. Magnetostatic and Mechanical Modelling

The shear operating mode of an MRFs is commonly utilised in rotary brakes. These actuators commonly take the form of a disc or a cylindrical housing as illustrated in Fig. 2. The magnetic flux Φ is applied orthogonally against the fluid shear. For disc brakes (Fig 2(a)), the fluid is confined in a thin volume placed perpendicular to the rotation axis while in the case of a cylindrical brake (Fig 2(b)), the fluid is in a cylindrical gap around the axis of rotation. The magnetic field is usually provided by coils. Thereby the resistive torque generated by the brake can be controlled by setting the coil current strength.

According to the Bingham model, an MRF brake displays a controllable torque T_h, which is a function of the field dependent yield stress, and a viscous torque T_v proportional to the relative velocity of the poles. The total braking torque is $T_b = T_h + T_v$.

In order to maximize the torque in a given volume, the association of many elementary discs or cylinders in parallel is an efficient way for achieving high levels of torque as presented in [5][15][17]. While in a multiple disc brake the relation between the number of discs and the torque is linear, the torque displayed by a multiple cylinder increases with the square of the radius of each cylinder.

A simplified structure scheme of the chosen brake geometry is presented in Fig. 3. The brake is composed of m fluid gaps.

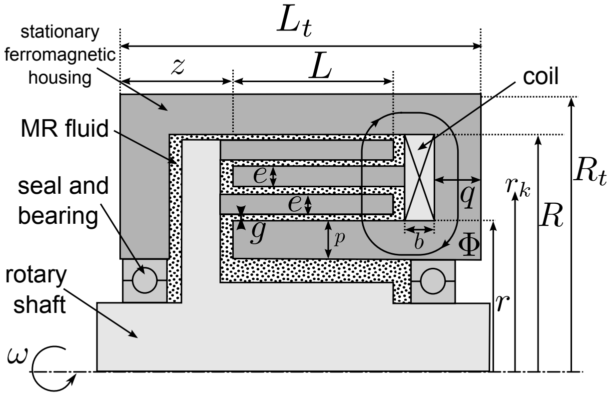

Fig. 3. Multilayered cylindrical brake with 4 fluid gaps: The external length and radius are L_t and R_t. Each cylinder separated by a gap g has a thickness e and a radius r_k. The radius of the smallest fluid gap is called r and the radius of the largest one is $r_4 = R$. L is the gap length, b the height of the coil and q the width of the ferromagnetic path on the right side of the coil, in-where the magnetic flux Φ loops. The width of the ferromagnetic section under the gaps is denoted p and of the lateral supports is z. The shaft rotates according to a velocity ω. The coil is reported laterally to the cylinders to reduce the electric consumption.

The total radius and length are R_t and L_t respectively. We denote g the fluid gap depth, e the thickness of each cylinder, r_k the inner radius of the fluid gap k, so that $1 \leq k \leq m$ with $k \in \mathbb{N}^*$, with $r_m = R$ and $r_1 = r$ the inner radius of the largest and of the smallest fluid surface respectively, b the coil width, q the width of the ferromagnetic path on the right side of the coil, and p the ferromagnetic path width below the gaps. The coil is placed adjacent to gaps in order to maximize the fluid surface crossed by the magnetic flux and to minimize its electric resistance.

The magnetic flux $\Phi(t)$ generated by a coil with N turns of wire excited by a current $i(t)$ is given by $\Phi(t) = Ni(t)/\mathscr{R}$, where $\mathscr{R}$ is the magnetic reluctance observed by the coil. The inner surface S_k of each fluid gap is $S_k = 2\pi L r_k$ with L the cylinder length and $r_{k+1} = r_k + e + g$. Considering only the reluctance of a fluid with an absolute permeability μ_{mr}, the reluctance is computed as follows:

$$\mathscr{R} = \frac{1}{2\pi\mu_{mr}L}\int_{r}^{R}\frac{dr}{r} = g\frac{ln\left[1+m(e+g)r^{-1}\right]}{2\pi\mu_{mr}L(g+e)} \qquad (3)$$

Considering that the permeability of the fluid is constant, a linear relationship between the magnetic field $H(t)$ and the magnetic flux density can be established as $B(t) = \mu_{mr}H(t)$. The induced magnetic field over the fluid surface is $H(t) = Ni(t)/\mu_{mr}S\mathscr{R}$ under assumption of a homogeneous flux on the fluid gap and non-saturation of the ferromagnetic circuit.

Regardless of the given geometry, the tangential resistive force is calculated by integrating $\tau(\dot{\gamma}, H)$ over the shearing surface S. For a rotary device, taking into account the radius r_k between this surface and the rotation axis, the braking torque T_b for m fluid gaps is the given by the sum of the torque delivered by each fluid surfaces as:

$$T_b = \sum_{k=1}^{m}\int\int r_k\tau(H,\dot{\gamma})dS \qquad (4)$$

The relationship between the magnetic field $H(t)$ and the fluid dependent yield stress $\tau_y(H)$ is typically denoted $\tau_y(H) = \alpha H(t)^\beta$ [9] where α and β are fluid constants. Before the saturation point of the fluid we consider $\beta = 1$. Using the Bingham plastic model integrated over each fluid surface combined to Equation 4, the total torque T_b is:

$$T_b = \frac{N\alpha}{\mathscr{R}\mu_{mr}}i(t)\sum_{k=1}^{m}r_k + 2\pi\frac{\eta L}{g}\omega(t)\sum_{k=1}^{m}r_k^3 \qquad (5)$$

With $\omega(t)$ the rotational velocity and η the fluid viscosity. In equation 5, the first term corresponds to the field dependent torque T_h and the second to the viscous torque T_v. The fluid gap length L is taken into consideration in the magnetic reluctance. The controllable torque can be rewritten as a function of the number of fluid gaps m and as a function of a desired magnetic flux density over the smallest fluid surface S_1 called B_d, as:

$$T_h = 2\pi r^2 L\frac{\alpha}{\mu_{mr}}\left[m + \frac{(m-1)(R-r)}{2r}\right]B_d \qquad (6)$$

This equation suggests that the controllable torque increases with the number of fluid gaps. The viscous torque T_v is obtained as the sum of the viscous torque of each cylinder and can be approximated by:

$$T_v = 2\pi\frac{\eta L r^3}{g}m\left[1 + \frac{3}{2}\left(\frac{e+g}{r}\right)(m-1)\right]\omega(t) \qquad (7)$$

The viscous torque quadratically increases with the number of fluid gaps.

The required flux to obtain the desired magnetic flux density B_d over the smallest fluid surface S_1 is $\Phi = B_d S_1$. This defines the magneto-motive force Ni_{max}, given by:

$$Ni_{max} = B_d S_1 \mathscr{R} \qquad (8)$$

where i_{max} is the necessary current to achieve B_d with N wire turns. The magnetomotive force then defines the power supply P. The power can be obtained by Joule's losses as $P = i_{max}^2 R_e$ where R_e is the electric resistance of the coil. The resistance expressed as a function of the resistivity of the wire κ, the mean radius of the coil r_b and the section of the wire S_w, is $R_e = 2\pi r_b \kappa N/S_w$. The section of the wire can be refereed to the desired maximum current-to-surface ratio ν in term of A/m^2 so that $i_{max} = S_w\nu$.

Replacing the current and the resistivity of the wire in the Joule's equation, the power can be rewritten as $P = 2\pi r_b\kappa\nu Ni_{max}$. Combining this equation with Equations 8 and 3, the power can be given as a function of the number of fluid gaps and the desired magnetic flux density on the smallest fluid by:

$$P = \pi\frac{\nu\kappa}{\mu_{mr}}g\frac{r_b r}{e+g}ln\left[1 + \frac{m(e+g)}{r}\right]B_d \qquad (9)$$

The power consumption increases with the number of fluid gaps and is dependent on the fluid gap depth.

The eletric time constant of the coil is a function of the magnetic reluctance [8]. Considering the coil as an LR circuit, the time constant is given by $\delta t_c = L_{in}/R_e$ where L_{in} is the inductance of the coil calculated as $L_{in} = N^2/\mathscr{R}$. The eletric time constant yields:

$$\delta t_c = \frac{N^2}{R_e\mathscr{R}} = \frac{B_d S_1}{2\pi\kappa\nu r_b} = 2\frac{rL}{\kappa\nu(R+r)}B_d \tag{10}$$

According to this equation, as $R = r + (e+g)m$ the electric time constant decreases with the number of fluid gaps. Knowing the power supply and the magnetic flux, the other geometrical dimensions of the brake can now be calculated.

The coil volume can be expresses as $V_{coil} = 2\pi r_b S_w N/\chi$ where χ is the coil fill rate or as a function of the power supply as $V_{coil} = P/\kappa\nu^2\chi$. Considering that the inner and the external radius of the coil are r and R respectively, the coil width b can be computed as $b = P/\pi(R^2-r^2)\nu^2\kappa\chi$, or rather:

$$b = \frac{g(R-r)}{\mu_{mr}\nu\chi(e+g)(R^2-3r^2)} ln\left[1+\frac{m(e+g)}{r}\right]B_d \tag{11}$$

The magnetic path must be dimensioned in order to support the magnetic flux $\Phi = B_d S_1$. A minimal ferromagnetic path section is therefore necessary to avoid the saturation of the path. Consider B_{fer} the maximal admissible magnetic flux density of the ferromagnetic path and S_n the ferromagnetic section crossed by the flux. The flux conservation gives the relation $B_d S_1 = B_{fer} S_n$ under the assumption of no flux leakages.

The minimal external radius to obtain the necessary cross section width on the top of the coil $R_t - R$, then is $R_t = \sqrt{2rLc_{sat} + R^2}$ whit $c_{sat} = B_d/B_{fer}$. The width q of the right side of the coil is obtained as $q = Lc_{sat}$. The ferromagnetic path over the fluid gaps must respect $p \leq r - \sqrt{r^2 - 2Lc_{sat}}$.

The total length of the brake is $L_t = z + b + L(1+c_{sat})$ with z the width of the lateral supports. The total volume is:

$$V = \pi[2rLc_{sat} + R^2][z + b + L(1+c_{sat})] \tag{12}$$

From these equations the cost functions for optimizing the brake are described in the next section.

C. Evaluation Criteria

The actuator is designed to fit a haptic feedback device. Haptic devices are robotic systems that display force or tactile sense to human operators which recreates the interaction with a virtual or teleoperated environment [21]. These devices need actuators able to cover a wide range of forces varying ideally from near to zero to near to infinite output impedance [19] [20]. An actuator adaptable for haptic devices should posses a high torque density, sufficient bandwidth, low output impedance, and high force display capability [3].

The cost functions for the optimization of the actuation system then deal with these three main requirements: the torque density, the controllability and reactivity.

The torque density symbolizes the maximization of the controllable torque for a given volume so that $\rho = T_h/V$ and is expressed in terms of N/m^2 as follows:

$$\rho = \frac{\alpha}{\mu_{mr}} \frac{rL[2rm + (m-1)(R-r)]}{(2rLc_{sat} + R^2)[L(2c_{sat}+1) + b]} B_d \tag{13}$$

TABLE I
INVARIANT PARAMETERS IN THE ANALYTIC MODEL

Term	Value	Unit	Parameter
B_d	0.7	T	desired induction in the smallest fluid gap
B_{fer}	1.5	T	maximal admissible induction of the path
μ_{mr}	$4.4\pi 10^{-7}$	H/m	fluid absolute permeability
μ_{fer}	∞	H/m	path absolute permeability
α	0.22	Pa.m/A	fluid magnetic field to yield stress constant
η	63.10^{-3}	Pa.s	fluid viscosity coefficient
ν	10.10^6	A/m^2	coil wire current to surface ratio
κ	17.10^{-9}	Ω/m	coil wire resistivity
χ	70%	-	coil fill rate

From this equation it can be concluded that ρ increases with the number of fluid gaps and can be improved using gaps with relative large radius r_k and small length L.

The controllability K depends on the dimension of the brake as well as the seals and bearings and is defined as the achieved controllable torque T_h at B_d divided by the viscous torque coefficient $T_v/\omega(t)$. It describes the ability of the brake to vary from low to high output impedance and is computed as $K = T_h\omega(t)/T_v$:

$$K = \frac{\alpha}{\mu\eta}\frac{g}{r}\left[\frac{2r + (m-1)(e+g)}{2r + 3(m-1)(e+g)}\right]B_d \tag{14}$$

This equation demonstrates that the controllability monotonically decreases with m. The controllable torque is expressed as a function of the desired induction and as a consequence, it is independent of the fluid gap depth. As the gap increases, the controllability increases too. However, the necessary power supply to achieve B_d raises. Since the controllability as well as the power supply increased with g, it represents a tradeoff between the power and the viscous torque.

Reactivity deals with the rapidity of the actuator to deliver a desired torque and depends on the response time of the electromagnetic circuit δt_c as well as the response time of the fluid. The mechanical response time of an MRF is typically inferior to a millisecond [25] and can be neglected compared to δt_c. Thus, the reactivity δt, is defined as the ratio controllable toque-to-electric time constant in terms of Nm/s, so that $\delta t = T_h/\delta t_c$, and is computed as:

$$\delta t = \pi\frac{\alpha\nu\kappa}{\mu_{mr}} r(R-r)\left[m + \frac{(m-1)(R-r)}{2r}\right] \tag{15}$$

The reactivity increases with the number of fluid gaps. Besides, this equation highlights that a large coil radius improves the reactivity but also increases the power supply.

III. OPTIMIZATION AND FINITE ELEMENT ANALYSIS

The magnetostatic model has been implemented in Matlab and finite element analysis (FEA) using FEMM software [1] is used to strengthen the analytical approach.

The employed fluid is the MRF122EG from Lord Corporation. The ferromagnetic path is made of pure iron (Telar 57).

---

[1] Finite Element Method Magnetics: www.femm.info

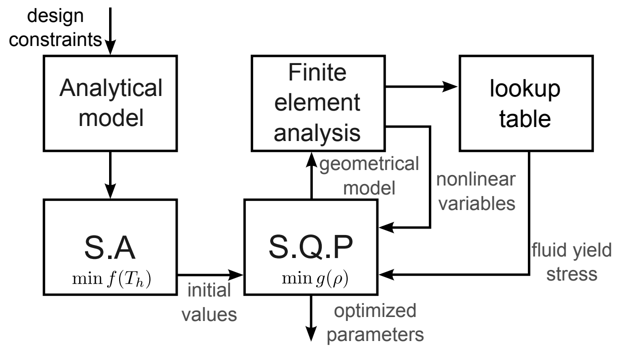

Fig. 4. Representation of the optimization algorithm. The geometrical constrains are implemented in the analytic model. An initial solution is found using the simulated annealing (SA) algorithm. The SA minimizes the function $(T_h-\hat{T})/\hat{T}$ where $\hat{T}$ in order to guarantee a required torque $\hat{T}$. The initial solution provided by the SA is sent to the sequential quadratic programming (SQP) algorithm which generates a finite element analysis to calculate nonlinear behaviours. The materials characteristics are taken in account using a lookup table. The SQP minimizes the function $1/\rho$ in view of maximizing the torque density. As output are determined m, L, r_k, Ni_{max}, q, T and r_b.

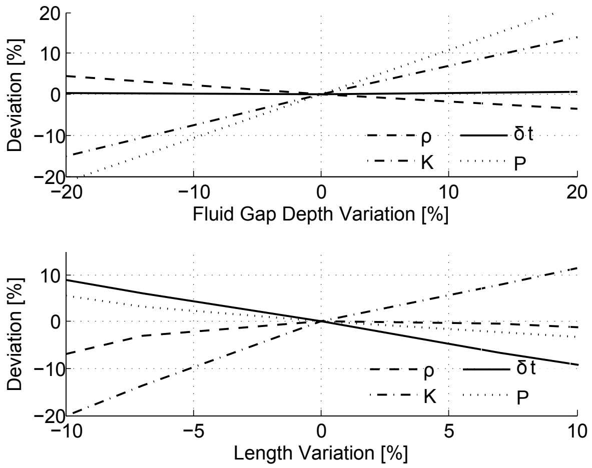

Fig. 5. Influence of the fluid gap depth g and of the fluid gap length L on the evaluation criteria. A compromise between ρ and K can be observed. If the fluid gap is increased from 0.5 mm to 0.6 mm (+20%), K increases by 14%. In the second figure, for $L=7$ mm, ρ reaches its maximum value. For a length variation superior to +7%, the ferromagnetic path on the right side of the coil is saturated. For variation inferior to -11%, a 6 mm radius hollow shaft can not be built.

Table I lists the parameters of the fluid, the ferromagnetic path and the coil adopted in the simulations. In the analytical model the absolute permeability of the fluid μ_{mr} and the field-to-yield stress constant α are assumed as constant. The permeability of the ferromagnetic path μ_{fer} is considered as infinite. The same parameters are used in the FEA except the B-H curves (magnetic flux density *versus* induced field) of the fluid and ferromagnetic material which are acquired from the datasheets of each material. In the same way, by contrast to the analytical model, in the FEA the fluid yield stress $\tau_y(H)$ is obtained as a non-linear function of the magnetic field.

The design specifications, the geometrical constraints and the optimisation variables used in the optimization algorithm are listed bellow.

Design specifications: The minimal required controllable braking torque is 3.2 Nm. In view of implementing the brake in a existing haptic device, a hollow shaft of 6 mm radius must be predicted and the external radius R_t must be inferior to 30 mm. Due to manufacturing limitations and to avoid the demormation of the cylinder, the thickness of each cylinder is set to $e=1$ mm. The emplacement of bearings and seal imposes $r-q\geq 13$ mm.

Geometrical constraints: In order to avoid saturation of the ferromagnetic path, the following geometric constraints must be respected. To avoid saturation on the top of the coil: $R_t\geq\sqrt{2rLc_{sat}+R^2}$. On the adjacent section of the coil the minimal width is $q\geq c_{sat}L$. Finally, the ferromagnetic path under the gaps necessitates $p\leq r-\sqrt{r^2-2Lc_{sat}}$.

Optimisation variables: The following parameters are the model variables: the number of fluid gaps m, the inner radius r of the smallest fluid gap, the fluid gap depth g, the length L of each fluid gap, and the means radius of the coil r_b.

Two critical parameters for optimising the brake are the fluid gap depth g and the number of fluid gaps m. The reactivity and the torque density are maximized when m tends to infinite. However, in order to maximize the controllability, m tends to zero. In the same way, the functions ρ, K, and δt do not meet an optimal value as a function of g. Maximising the torque density necessitates the minimization of the fluid gap depth, while maximising the controllability implies a large fluid gap. Consequently, g determines the compromise controllability *versus* power supply and controllability *versus* torque density. Hence, g is choose to be set at 0.5 mm and optimisation will focus on the maximization of the torque density.

The optimization algorithm represented in Fig. 4 comprises two successive steps. In the first step, a solution with respect to the geometric specifications and constraints is obtained using a "simulated annealing algorithm" (SA). It consists of a random search algorithm which statistically guarantees the convergence of the model to the required torque $\hat{T}$ after a finite number of iterations. The SA minimizes the following function:

$$f(T_h)=\frac{|T_h-\hat{T}|}{\hat{T}} \tag{16}$$

The results provided by the SA are used in the "sequential quadratic programming" (SQP) algorithm which searches for an optimal solution that maximises the torque density. The solution provided by the SA algorithm guarantees that the SQP does not converge to a local minimum.

In order to maximize the torque density, the SQP minimizes the function $g(\rho)$:

$$g(\rho)=\frac{1}{\rho} \tag{17}$$

The SQP communicates with the FEA software in order to take into account all magnetic saturation and non-linearities. The magnetic field is monitored for 10 levels of current strength varying from 0 A to 1 A. Results were obtained four fluid gaps. The smallest one has 22.5 mm radius, as a consequence the other have 24 mm, 25.5 mm and 27 mm respectively. The optimal fluid gap length is 7 mm.

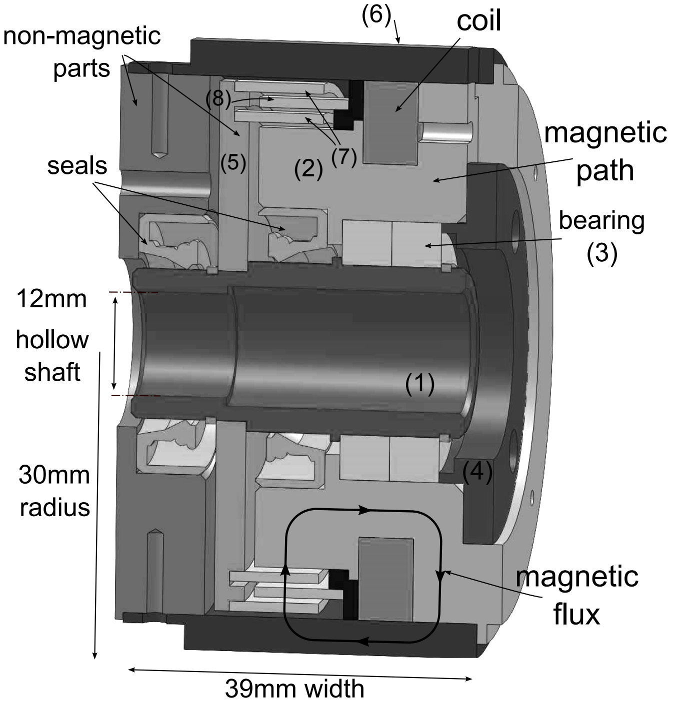

Fig. 6. CAD cross-view of the MRF-brake. Attached to the hollow rotary shaft (1) a thin non-magnetic cylinder (5) supports two ferromagnetic cylinders which compose the fluid chamber. The coil is into the inner core (2) and thanks to the external housing (6), the magnetic flux is guided across the fluid gaps. A non-magnetic lateral support (4) blocks the translation of the axis and bearings. The brake has 30 mm radius with a 6 mm radius hollow shaft and 39 mm length. The expected torque in the linear range is 3.4 Nm.

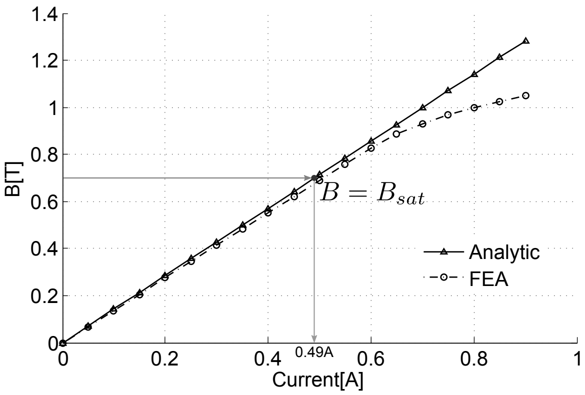

Fig. 7. Magnetic flux density over the smallest fluid surface as a function of the current. Using the analytical model, the surface reaches the desired induction of 0.7 T at 0.49 A and at 0.52 A using the finite element analysis model. As speficied in the model, this is the maximal current in the norminal regime.

TABLE II
OPTIMIZED BRAKE DIMENSIONS

term	value	unit	parameter
m	4	-	number of fluid gaps
r	22.5	mm	smallest fluid gap radius
r_2	24	mm	second fluid gap radius
r_3	25.5	mm	third fluid gap radius
r_4	27	mm	fourth fluid gap radius
L	7	mm	fluid gap length
g	0.5	mm	fluid gap depth
r_b	23.5	mm	coil mean radius
R_t	30	mm	outer radius

The fluid gap depth and the length of the gaps have an important influence on the performance of the brake. Increasing the length improves the torque but also the necessary power supply and the dimensions of the magnetic path. An optimal fluid gap length that maximizes the torque density can be found. With regard to the fluid gap depth however, the evaluation criteria do not present an maximal value as presented in Fig. 5. A small change on these dimensions affects strongly the performance.

The design of the brake is shown in Fig. 6. The final external dimensions are 39 mm width, 30 mm radius with 6 mm hollow shaft radius. The rotary hollow shaft (1) is connected to the stationary ferromagnetic path (2) using two bearings (3). A bearing cap (4) constraints their motion along the axis. Around the shaft (1) is placed a thin rotary disc (5) which supports the rotary cylinders (7) of the fluid chamber. The rotary parts are (1) and (5). All but (2)(6)(7)(8) are non magnetic parts. By this means the magnetic flux is guided into the fluid gaps while minimizing flux leakages.

The brake is designed to function with a maximum required magnetic flux density B_d over the smallest fluid surface S_1. Figure 7 shows the evolution of the mean induction value over S_1 as a function of the current. According to the analytical model, the desired induction is reached for a magnetomotive force of Ni_{max} =232 A.turn. It is achieved with 475 turns of 0.25 mm diameter wire and 0.49 A. According to the adopted current to surface ratio, this correponds to the maximal current in norminal regime. Beyond this point, the fluid is expected to saturate. Therefore, this is the limit of validity of the analytical model. Using the FEA model, the desisted induction is attained at Ni_{max}=247 A.turn or rather 475 turns of wire and 0.52 A. This represents an error of +6% compared to the analytical model (or 6% less torque for Ni_{max} =232).

Fig. 8 presents the simulation results using the FEA. The magnetic flux density B across the ferromagnetic circuit for Ni_{max}=247 A.turn is show in Fig. 8(a). Both the fluid and the ferromagnetic path reach their saturation at the same magnetomotive force. Fig 8(b) presents the induction and the field over each fluid surface. The expected torque using the FEA combined to the Bingham model is 3.2 Nm, which corresponds to the reference torque used in the optimization. Using the analytical model, the estimated torque is 3.4 Nm. The largest surface reaches its saturation at 0.9 A.

The optimal value obtained using the optimization algorithm are listed in Table II. Using these parameters, the brake has been built and characterized. The experimental results are presented in the next section.

IV. EXPERIMENTAL RESULTS

The optimized brake has been built using aluminium for the non-magnetic parts and pure iron (Telar 57) for the magnetic path. The sealing of the fluid is ensured using low-friction radial shaft seals without spring compressors.

The test bench of Fig. 9 is used to characterise the brake. A Maxon motor RE-40 linked to a reduction stage of 50:1 that can apply 6 Nm is used to generate a velocity. The

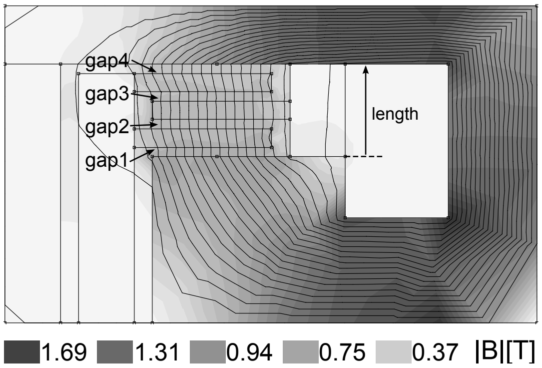

(a) Finite element simulation

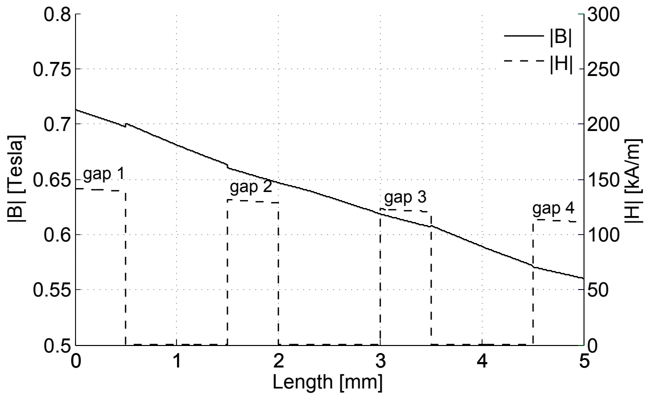

(b) Magnetic field and magnetic flux density

Fig. 8. Simulation results using finite element analysis. In (a) the magnetic flux density in the ferromagnetic path. The ferromagnetic path and the fluid reach their saturation at the same magnetic flux. The evolution of the induction across the fluid gaps is shown in (b). The fluid is exploited up to the desired induction of 0.7 T at 0.52 A.

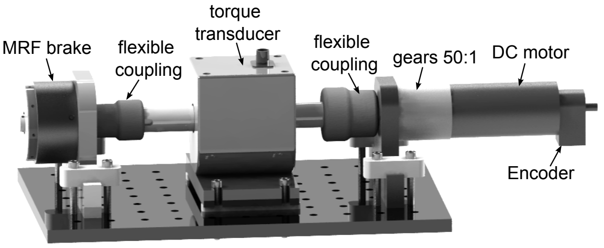

Fig. 9. Experimental test bench. The brake is connected to an excitation motor Maxon RE-40 through a torque transducer Sensors Development 01324. The motor is connected to a reduction stage with a reduction ratio of 50:1 and can apply a torque of 6 Nm. The position is measured using an incremental encoder with 500 ppr.

gearmotor is connected to the brake through a torque transducer Sensor Development (model 01324). The position of the shaft is measured using an incremental encoder with 500 pulses per revolution. The brake and the motor are controlled by a discrete controller (Silabs 8051F120) with a sampling frequency of 16 kHz and a linear power amplifier. The braking torque, the current of the brake and the velocity of the shaft are recorded at 2.5 kHz.

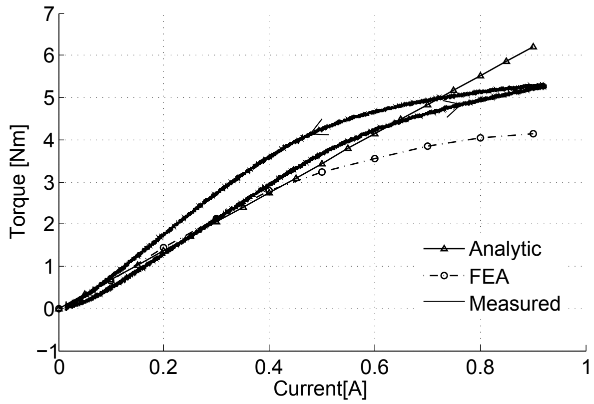

Fig. 10. Measured braking torque with its hysteresis loop. The expected torque and the measured torque when the fluid reaches the desired induction are 3.4 and 3.6 Nm respectively according to the analytical model. Using the FEA, the expected torque is 3.2 Nm and the measured torque is 3.8 Nm. The experimental results overreach theory by +5.5% and +15.7% compared to the analytical and to the FEA models respectively. When the largest fluid surface reaches B_d, the torque is 5.3 Nm. The velocity varies from 0.9 to 0.5 turn/sec which corresponds to a viscous torque at zero field inferior to 4mNm.

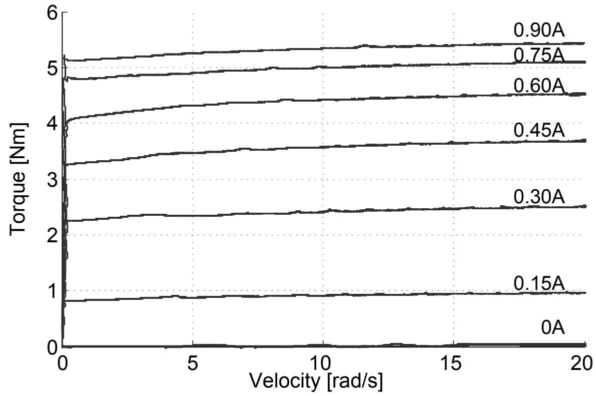

Fig. 11. Influence of the velocity on the braking torque. The brake is activated according to different current strengths varying from 0 A to 0.9 A. For each current, the velocity of the motor is gradually increased using the controller.

Fig. 10 presents the measured and estimated braking torques. The motor is activated and an excitation current is sent to the brake. The current calculated by the controller is a triangular form 0 A to 900 mA to 0 A according to slope of 1 mA/10ms. The measured torque at the desired induction of the fluid according to the analytical and finite element models at 0.49 A and 0.52 A are 3.6 Nm and 3.8 Nm respectively. When the largest surface reaches B_d (at 0.9 A) the measured torque is 5.3 Nm. The torque at zero field is 30 mNm.

As presented in the rheological model of Equation 1, the viscosity of the fluid generates an uncontrollable torque. In Fig. 11, the influence of the velocity on the braking torque is presented. The brake is activated with constant currents ranging from 0 A to 0.9 A with 0.15 A steps. The motor velocity is then gradually increased. Using Equation 7 the estimated viscous torque coefficient at zero field is $T_v = 324$ μNms. The measured viscous friction coefficient is $T_v = 567$ μNms. This represents an error in the estimation of the viscous torque coefficient of -59%. The influence of the viscous torque is negligible compared to the controllable torque.

The electric response of the coil is presented by its bode diagram in Fig. 12. The bode diagram is obtained using an excitation sinusoidal voltage of 12 V with a sweep frequency

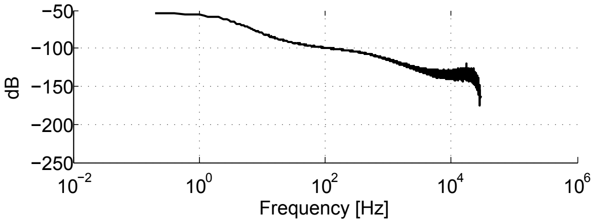

(a) Voltage to current gain

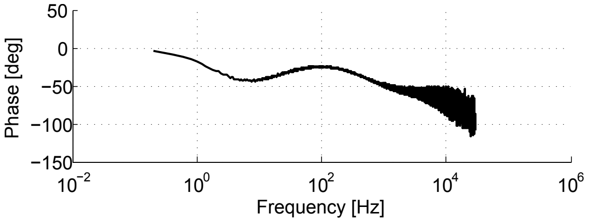

(b) Voltage to current phase

Fig. 12. Frequency respose of the brake. A 10 s sinusoidal sweep frequency of a 12 V varing from 0.1 Hz to 30 kHz is sent to the brake and the current is measured by a shunt resistance of 1 Ω. The observed cut frequency is 18 Hz.

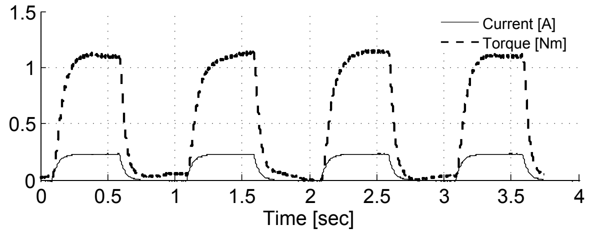

Fig. 13. Electromechanical response. The figure presents the brake response for 1 Hz a step-type voltage excitation using a linear amplifier. The mechanical response time for a voltage step is 200 ms. The response time of the fluid can be neglected compared to the electromagnetic respose time.

form 0.1 Hz to 30 kHz and by measuring the induced current with a shunt resistance of 1 Ω. The observed cut frequency at $\pi/4$r ad out of phase is 18 Hz. The observed electromagnetic bandwidth of the brake is given by a step time excitation voltage. According to Equation 10, the expected time constant is 51.7 ms. Considering that the response time is $4\delta t_c$, this yields a theoretical response time of 204 ms. In Fig. 13 the mechanical response for a 5 V excitation voltage with a frequency of 1 Hz in open-loop is presented. The observed electromechanical response time is 200 ms. This result comprises the response time of the fluid.

A. Discussion

The torque calculated by the analytical model when the smallest fluid surface reaches the desired induction, corresponding to 0.49 A, is 3.4 Nm. For the same current, the measured torque is 3.6 Nm. This result overreaches the theory by +5.5%. After this point, the fluid is supposed to saturate and the analytical model is not valid. According to the FEA, the smallest fluid surface reaches B_d at 0.52 A and the expected torque is 3.2 Nm, which corresponds to the desired torque in the optimization algorithm. The measured torque at this current is 3.8 Nm. It represents a deviation of +15% compared to the FEA.

The deviation can be amounted to three main phenomena.

1) It has been shown in Fig. 5 that the fluid gap depth has a strong influence on the power supply. A variation of 10% of the gap depth implies a change of 11% in the power. A small variation of the fluid gap strongly alters the necessary magnetomotive force Ni_{max} to achieve B_d. Therefore, due to the dimensional tolerance of the cylinders al well as assembly imprecisions, the reluctance may be lower than expected. For example, an imprecision in the positioning of the cylinders, that increases the fluid gap length of 0.1 mm, leads a decrease of 1.27% on the total reluctance which results in 1.42% more torque.
2) The analytical model assumes a homogeneous magnetic field over a fluid gap. However, the FEA presented in Fig. 8(b) highlights that the magnetic flux density is not constant and is stronger in the vicinity of the coil as compared to elsewhere. As a consequence, the fluid reacts with different yield stress in different locations within the same fluid gap which contributes to the observed deviation.
3) Up to the desired induction, the relation between the yield stress and the magnetic field $\tau_y(H) = \alpha(H)^{\beta}$ is assumed as linear ($\beta = 1$). This imprecision contributes to the observed deviation since for most MR fluids the index β is comprised between 1 and 2 before saturation. In the same way, when the largest fluid surface reaches B_d at 0.9 A, the torque calculated by the FEA is 4.14 Nm. Compared to the measured torque, a deviation of 47% is observed. The deviation between the FEA and the measured torque increases when the theoretical saturation point of the fluid is exceeded. In the proposed magnetostatic model, the torque as well as the power supply are strongly dependent on the permeability of the fluid as shown in Equations 6 and 9 respectively. Therefore, this deviation may be due to imprecisions in the estimation of the permeability of the fluid beyond the saturation point as well as the estimation of field dependent yield stress as a function of the applied field. The estimated yield stress $\tau_y(H)$ is given by the fluid's manufacturer as guidelines only.

V. CONCLUSION

In this paper a new magnetostatic approach to design an MRF brake is proposed. The magnetic circuit is dimensioned to deliver a desired magnetic flux density over the smallest fluid surface. This enables the brake to maintain the fluid under its saturation point in order to guarantee a linear current-torque relationship and to minimize the power supply. In addition, considering a maximal admissible induction attributed on the ferromagnetic path, the circuit is designed so that the fluid and the path reach their saturation for the same magnetic flux. By this means the volume of the path can be optimized. The brake is shown in Fig. 14.

The considered evaluation criteria are the torque density, the controllability and the reactivity, as a function of the number of fluid gaps and the shearing surface dimensions.

TABLE III
SPECIFICATIONS OF THE PROPOSED BRAKE AND COMPARISON TO OTHER DOCUMENTED RESULTS

	unit	Designed brake	Lord Corp. RD-2078-1	Senkal and Gurocak [22]	Liu et al. [11]	Guo and Liao [6]	Nam et al. [12]
Max. Torque	Nm	5.3	4.0	10.9	7	0.48	4.2
Off-state	mNm	30	400	100	500	50	-
Length	mm	39	35.7	89.7	21	18	38
Radius	mm	30	96.6	31.75	78	25	60
Power	W	19	15	20	-	-	52
Time Const	ms	50	10	60	-	25	33
Torque/Vol	kN/m^2	48.1	12.5	38.3	17.4	13.6	9.8
Efficiency	mNm/W	280	260	540	-	-	80
Controll.	-	176	10	109	14	9.6	-
Reactivity	kNm/s	106	400	108	-	19.2	127

The analytical model highlights that the torque density and the reactivity increase with the number of fluid gaps, while the controllability is inversely depended to it. It can be concluded that the torque density can be improved using gaps with relative large radius compared to the length. In particular, the fluid gap depth plays an important role with regards to the controllability/torque density and controllability/power supply tradeoffs. These compromises have been established by setting the fluid gap to 0.5 mm and by focusing on the optimization of the torque density.

The optimization algorithm uses both a simulated annealing algorithm (SA) quential quadratic programming algorithm (SQP). The SA looks for a geometrical solution and guarantees a minimal torque of 3.2 Nm. This algorithm is necessary to avoid the convergence to a local minimum of the second algorithm. Subsequently, the SQP maximizes the torque density using this equation as cost function. When exploited up to its complete saturation, the brake can generate 5.3 Nm with 19 W power consumption. This gives a torque density of 48.1 kN/m^2, a maximum-to-minimum torque ratio, taking into consideration the coulomb friction, of 176 and a torque-to-time constant of 106 kNm/s.

Table III compares the design specifications of the proposed brake to a commercially available brake and some of brakes available in the literature. The designed brake provides 23% more torque for a volume 76% inferior capared to the commercial brake but the reactivity is 4 times inferior.

The developed magnetostatic model needs only three inputs to completely define the brake: the number of fluid gaps, the inner radius of the smallest fluid gap and the fluid gap depth. It is designed to provide a desired induction on the fluid gap regardless of the dimensions of the brake. By these means the saturation can be avoided and the behaviour remains in linear range, which sets the limit of the validity of the model. All other dimensions can be calculated accordingly in order to accurately guide the magnetic flux into the gaps without saturation.

The relatively low differences observed between the model and the experimental results in the linear range indicates that this approach is sufficient to design a multiple cylinder MRF brake. Moreover, the high controllability and torque capability make the actuator amply adaptable for high transparency human-machine interfaces design.

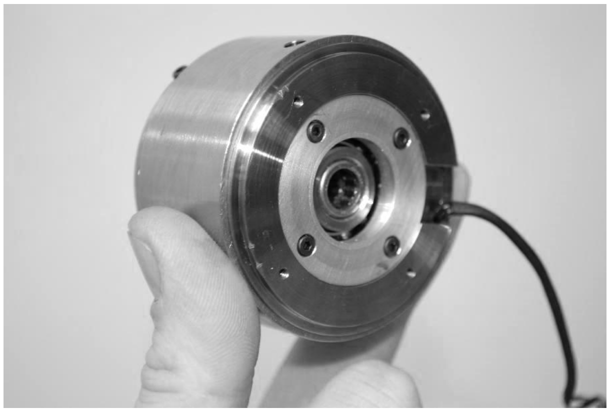

Fig. 14. View of the compact 5.3 Nm MRF brake. The actuator possesses a torque density of 48.1 kN/m^2 and a maximal to minimal torque ratio of 176 with 50 ms time constant.

REFERENCES

[1] B. Assadsangabi, F. Daneshmand, N. Vahdati, M. Eghtesad, and Y. Bazargan-Lari. Optimization and design of disk-type mr brakes. *International Journal of Automotive Technology*, 12:921–932, 2011.

[2] David J. Carlson, Douglas F. Leroy, John C. Holzheimer, Donald R. Prindle, and Robert H. Marjoram. Controllable brake, January 1998.

[3] P. Fauteux, M. Lauria, M.-A. Legault, B. Heintz, and F. Michaud. Dual differential rheological actuator for robotic interaction tasks. In *Advanced Intelligent Mechatronics, 2009. AIM 2009. IEEE/ASME International Conference on*, pages 47 –52, july 2009.

[4] Junji Furusho, Masamichi Sakaguchi, Naoyuki Takesue, and Kenichi Koyanagi. Development of er brake and its application to passive force display. *Journal of Intelligent Material Systems and Structures*, 13(7-8):425–429, 2002.

[5] K H Gudmundsson, F Jonsdottir, and F Thorsteinsson. A geometrical optimization of a magneto-rheological rotary brake in a prosthetic knee. *Smart Materials and Structures*, 19(3):035023, 2010.

[6] Hongtao Guo and Wei-Hsin Liao. Optimization of a multifunctional actuator utilizing magnetorheological fluids. In *Advanced Intelligent Mechatronics (AIM), 2011 IEEE/ASME International Conference on*, pages 67 –72, july 2011.

[7] Kerem Karakoc, Edward J. Park, and Afzal Suleman. Design considerations for an automotive magnetorheological brake. *Mechatronics*, 18(8):434 – 447, 2008.

[8] Jeong-Hoi Koo, Fernando D Goncalves, and Mehdi Ahmadian. A comprehensive analysis of the response time of mr dampers. *Smart Materials and Structures*, 15(2):351, 2006.

[9] W.H. Li and H. Du. Design and experimental evaluation of a magnetorheological brake. *The International Journal of Advanced Manufacturing Technology*, 21:508–515, 2003.

[10] Jason Lindler and Norman M Wereley. Quasi-steady bingham plastic analysis of an electrorheological flow mode bypass damper with piston bleed. *Smart Materials and Structures*, 12(3):305, 2003.

[11] B Liu, W H Li, P B Kosasih, and X Z Zhang. Development of an mr-brake-based haptic device. *Smart Materials and Structures*, 15(6):1960, 2006.

[12] Yun-Joo Nam, Young-Jin Moon, and Myeong-Kwan Park. Performance improvement of a rotary mr fluid actuator based on electromagnetic design. *Journal of Intelligent Material Systems and Structures*, 19(6):695–705, 2008.

[13] Q H Nguyen and S B Choi. Optimal design of an automotive magnetorheological brake considering geometric dimensions and zero-field friction heat. *Smart Materials and Structures*, 19(11):115024, 2010.

[14] Quoc Hung Nguyen, Jun Cheol Jeon, and Seung Bok Choi. Optimal design of an hybrid magnetorheological brake for Middle-Sized motorcycles. *Applied Mechanics and Materials*, 52-54:371–377, March 2011.

[15] Jason Nikitczuk, Brian Weinberg, and Constantinos Mavroidis. Control of electro-rheological fluid based resistive torque elements for use in active rehabilitation devices. *Smart Materials and Structures*, 16(2):418, 2007.

[16] Edward J. Park, Luis Falco da Luz, and Afzal Suleman. Multidisciplinary design optimization of an automotive magnetorheological brake design. *Computers & Structures*, 86(35):207 – 216, 2008. Smart Structures.

[17] F. Periquet and J.Lozada. A miniature 1-dof mr fluid based haptic interface. *12th International Conference on New Actuators*, pages 541–544, 2010.

[18] C. Rossa, L. Eck, A. Micaelli, and J. Lozada. On a novel torque detection technique for magnetorheological actuators. *Sensors Journal, IEEE*, PP(99):1–1, 2013.

[19] Carlos Rossa, Jose Lozada, and Alain Micaelli. Stable haptic interaction using passive and active actuators. In *Robotics and Automation (ICRA), 2013 IEEE International Conference on*, 2013.

[20] Carlos Rossa, Jos Lozada, and Alain Micaelli. Interaction power flow based control of a 1-dof hybrid haptic interface. In Poika Isokoski and Jukka Springare, editors, *Haptics: Perception, Devices, Mobility, and Communication*, volume 7283 of *Lecture Notes in Computer Science*, pages 151–156. Springer Berlin Heidelberg, 2012.

[21] Carlos Rossa, Jos Lozada, and Alainn Micaelli. A new hybrid actuator approach for force-feedback devices. pages 4054–4059, 2012.

[22] Doruk Senkal and Hakan Gurocak. Serpentine flux path for high torque mrf brakes in haptics applications. *Mechatronics*, 20(3):377 – 383, 2010.

[23] Likang Yang, Fubin Duan, and Anders Eriksson. Analysis of the optimal design strategy of a magnetorheological smart structure. *Smart Materials and Structures*, 17(1):015047, 2008.

[24] H. H. Zhang, C. R. Liao, W. M. Chen, and S. L. Huang. A magnetic design method of mr fluid dampers and fem analysis on magnetic saturation. *Journal of Intelligent Material Systems and Structures*, 17(8-9):813–818, 2006.

[25] Chang Sheng Zhu. The response time of a magnetorheological fluid squeeze film damper rotor system. *Key Engineering Materials*, 334:1085–1088, 2007.